**Annales
Geophysicae**

A global MHD simulation of an event with a quasi-steady northward IMF component

V. G. Merkin[1], J. G. Lyon[2], B. J. Anderson[3], H. Korth[3], C. C. Goodrich[1], and K. Papadopoulos[4]

[1]Center for Space Physics, Boston University, Boston, MA, USA
[2]Department of Physics and Astronomy, Dartmouth College, Hanover, NH, USA
[3]The Johns Hopkins University, Applied Physics Laboratory, Laurel, MD, USA
[4]Department of Astronomy, University of Maryland, College Park, MD, USA

Abstract. We show results of the Lyon-Fedder-Mobarry (LFM) global MHD simulations of an event previously examined using Iridium spacecraft observations as well as DMSP and IMAGE FUV data. The event is chosen for the steady northward IMF sustained over a three-hour period during 16 July 2000. The Iridium observations showed very weak or absent Region 2 currents in the ionosphere, which makes the event favorable for global MHD modeling. Here we are interested in examining the model's performace during weak magnetospheric forcing, in particular, its ability to reproduce gross signatures of the ionospheric currents and convection pattern and energy deposition in the ionosphere both due to the Poynting flux and particle precipitation. We compare the ionospheric field-aligned current and electric potential patterns with those recovered from Iridium and DMSP observations, respectively. In addition, DMSP magnetometer data are used for comparisons of ionospheric magnetic perturbations. The electromagnetic energy flux is compared with Iridium-inferred values, while IMAGE FUV observations are utilized to verify the simulated particle energy flux.

Keywords. Magnetospheric physics (Magnetosphere-ionosphere interactions; Plasma convection; Solar wind-magnetosphere interactions)

1 Introduction

Global magnetohydrodynamic (MHD) models have become a valuable and robust tool for magnetospheric research in the past few years. Today they can make relatively accurate predictions of macroprocesses in the earth's magnetosphere, both qualitatively and quantitatively, while running at a fraction of real time with a reasonable resolution. The reliability

Correspondence to: V. G. Merkin
(vgm@bu.edu)

of such predictions is largely dependent on the validation of these models against available observations. In addition to improvements in robustness and reliability, validation of the models provides important insights into the physics of the system.

The problem with validating a global magnetospheric model arises from the immense scale of the earth's magnetosphere and the relative scarcity of observations. However, the situation in the ionosphere is much more favorable due to availability of different kinds of observations (ground-based magnetometers, radars, low-altitude satellites, etc.). The Iridium constellation data is especially advantageous for comparisons with global MHD simulations, since the large number of spacecraft enables simultaneous magnetic perturbation measurements that are effectively combined through a spherical harmonic fitting procedure into a global synoptic map of ionospheric field-aligned currents (FAC) (Anderson et al., 2000; Waters et al., 2001; Anderson et al., 2002).

For the purposes of this paper, simulations have been accomplished using the Lyon-Fedder-Mobarry (LFM) global MHD model (Lyon et al., 2004, and references therein). The earlier study comparing LFM simulations with Iridium observations (Korth et al., 2004) looked into moderate active time conditions and found that increasing the simulation resolution improved the intercomparison between simulations and observations. In addition, it was pointed out that the disparity between the observed and simulated field aligned currents was largely due to deficiencies in the LFM ionospheric conductance model. In contrast to that work, here we are interested in a situation with a strong northward component of the interplanetary magnetic field (IMF). For these conditions, the magnetic perturbation signatures and the corresponding NBZ current system appear at very high latitudes near the magnetic pole (e.g. Burke et al., 1979; Ijima et al., 1984; Zanetti et al., 1984) where there is usually no or very sparse radar and ground-based magnetometer coverage. On the other hand, the Iridium constellation consists of satellites

in circular, polar orbits and therefore there is no restriction on data coverage in the high-latitude regions. We are seeking to establish how well the model is able to capture main features of the ionospheric current distribution and convection pattern as well as energy input into the ionosphere during such conditions. This is useful, in particular, for identifying strengths and weaknesses of the LFM model, as well as other such models, in simulating realistic events driven by above-the-cusp magnetopause reconnection as opposed to the somewhat more investigated situation of the southward IMF driving. In addition, empirical models of ionospheric particle precipitation used in global MHD simulation codes have not been previously extensively tested, especially under weakly driven conditions. We use available observations of precipitating particle energy and flux to examine the performace of such an empirical calculation employed in the LFM model.

In this paper we concentrate on the event previously studied using Iridium data (Korth et al., 2005). The event occurred on 16 July 2000, the day after the Bastille Day Storm. The IMF B_Z component remained substantially northward throughout that day and fairly steady for at least 3 h. In addition to Iridium spacecraft, data were available from the plasma drift meters and magnetometers onboard the Defense Meteorological Satellite Program (DMSP) F13 and F15 satellites. We show comparisons of the ionospheric field aligned currents and electromagnetic energy flux input into the ionosphere between the LFM model and Iridium observations as well as the cross-track magnetic perturbations and drift velocities observed by the DMSP satellites. In order to investigate the possible effects of the simulation code resolution, the LFM was run using the lowest resolution – 53×24×32 cells (see Sect. 2) and the doubled angular resolution – 53×48×64. The lowest resolution LFM simulations were also complemented by the Coupled Magnetosphere-Ionosphere-Thermosphere (CMIT) model simulations (Wiltberger et al., 2004; Wang et al., 2004) to investigate the effects of the ionospheric conductance model. Finally, the precipitating particle energy measurements from DMSP spacecraft and particle flux measurements from the far-ultraviolet (FUV) instrument onboard the IMAGE spacecraft were used to validate the precipitation model within the LFM and CMIT models for this period of northward IMF.

2   Simulation methods

The most recent and exhaustive description of the LFM model can be found in the work of Lyon et al. (2004). Here we outline the details pertinent to the present discussion. The LFM model simulation grid is a distorted spherical grid with the symmetry axis directed along the Solar Magnetic (SM) X-axis. The lowest resolution simulation code has dimensions 53×24×32 meaning that there are 53 cells in the radial direction and 24 and 32 cells in the polar and azimuthal direc-

tions (in the LFM sense), respectively. The resolution in the radial direction defines the location of the inner boundary of the MHD grid at ∼2 R_E, which places the low-latitude ionospheric boundary at ∼45° magnetic latitude. This provides an average resolution of about 3.75°×2.81° in the ionosphere, but it is nonuniform with a sparser resolution around the magnetic pole and convergent points on the day and night ends of the noon-midnight meridian (Wiltberger et al., 2004, Fig. 1). Usually, low-latitude spacecraft provide data with a much higher space and time resolution: DMSP plasma drift meter data, for instance, is available at a fraction of a degree resolution. Therefore, for comparisons presented in this paper we use the LFM simulation code version with the doubled angular resolution – 53×48×64. We have also run the single-resolution LFM simulation code to explore effects of the code resolution on the ionospheric field aligned current and electrostatic potential patterns.

The inner boundary condition of the LFM model follows from the current continuity and relates the electrostatic potential to the field aligned current through the height-integrated ionospheric conductivity (Fedder and Lyon, 1995; Fedder et al., 1995a; Lyon et al., 2004). The ionospheric conductance is calculated by an empirical model which first computes the EUV ionization contribution and then estimates the precipitating particle characteristic energy and flux from MHD macrovariables (Fedder et al., 1995b). As the description of the latter calculation will be needed in further discussion (Sect. 4.5), we outline here its relevant points. First, the initial guess is made about the particle characteristic energy and number flux at the inner boundary of the MHD simulation code:

$$E_0 = \alpha C_S^2 \tag{1}$$

and

$$\Phi_0 = \beta \rho E_0^{1/2}, \tag{2}$$

where C_S is the sound speed and ρ is the density of the MHD plasma, and α and β are empirical coefficients. Next, the above values are corrected to include effects of particle acceleration by field aligned electric fields:

$$E = E_0 + E_\parallel, \tag{3}$$

where (Chiu and Cornwall, 1980; Fridman and Lemaire, 1980; Chiu et al., 1981)

$$E_\parallel = \frac{R J_\parallel E_0^{1/2}}{\rho}, \tag{4}$$

$J_\parallel$ is the field aligned current, and R is another empirical coefficient. Finally, for downstreaming electrons

$$\Phi = \Phi_0 \left(8 - 7 \exp \frac{-E_\parallel}{7E_0} \right), \tag{5}$$

where $E_\parallel$ is a positive quantity. The precipitating electron energy and energy flux are then transferred into the ionospheric conductance according to the Robinson's formula (Robinson et al., 1987).

Recently, the CMIT model has been developed (Wiltberger et al., 2004; Wang et al., 2004), in which the LFM global magnetospheric model is coupled to the Thermosphere-Ionosphere Nested Grid (TING) model (Wang et al., 1999) that replaces the empirical calculation of the ionospheric conductances in the standalone LFM. At this time, the CMIT model can operate only at the lowest LFM resolution ($53\times24\times32$). Thus, we will not use the CMIT results for direct comparisons with data, but will use them to investigate possible effects of the ionospheric conductance model used.

3 Event description and inflow boundary conditions

For the purposes of this study we have chosen the event with sustained northward IMF that occurred on 16 July 2000. This event has been previously considered by the work of Korth et al. (2005) using data from Iridium, DMSP and IMAGE FUV. Here we use the same observations for comparisons with global MHD simulations.

The solar wind conditions as observed by the ACE satellite during the event are shown in Fig. 1. The two vertical solid lines mark the period between 16:00 UT and 19:00 UT during which the comparisons are made. As can be seen in the figure, the solar wind conditions remain fairly steady with a substantially large northward IMF component during this 3-h period. To perform the simulations, the solar wind was propagated to the earth with the time lag of 34 min determined by Korth et al. (2005). When represented in Geocentric Solar Magnetospheric (GSM) coordinate system, the solar wind is almost strictly anti-sunward while the IMF is almost due northward. The presence of the large dipole tilt angle leads to a considerable negative Z-component of the solar wind velocity in SM coordinates. In addition, there is a small but finite negative SM B_X as seen in Fig. 1.

It is a well-known problem in global MHD simulations that it is difficult to reconcile single-satellite time-dependent B_X observations with $\nabla \cdot \mathbf{B} = 0$ condition (e.g. Raeder et al., 2001, and references therein). In the case considered here (from 16:00 UT through 19:00 UT), B_X in SM coordinates is small but constitutes a significant fraction of the total magnetic field. This results in a significant tilt of the IMF from SM YZ-plane and makes it necessary to drive the simulations with the IMF having a non-zero B_X component. This problem is usually solved in the LFM simulation code by using a linear regression technique to represent B_X in the form $B_X = B_X^{(0)} + \alpha B_Y + \beta B_Z$, where the regression coefficients $B_X^{(0)}$, α, and β define the plane of the front to which the unknown 3-D-structure of the solar wind is reduced (there are also methods that use multiple spacecraft
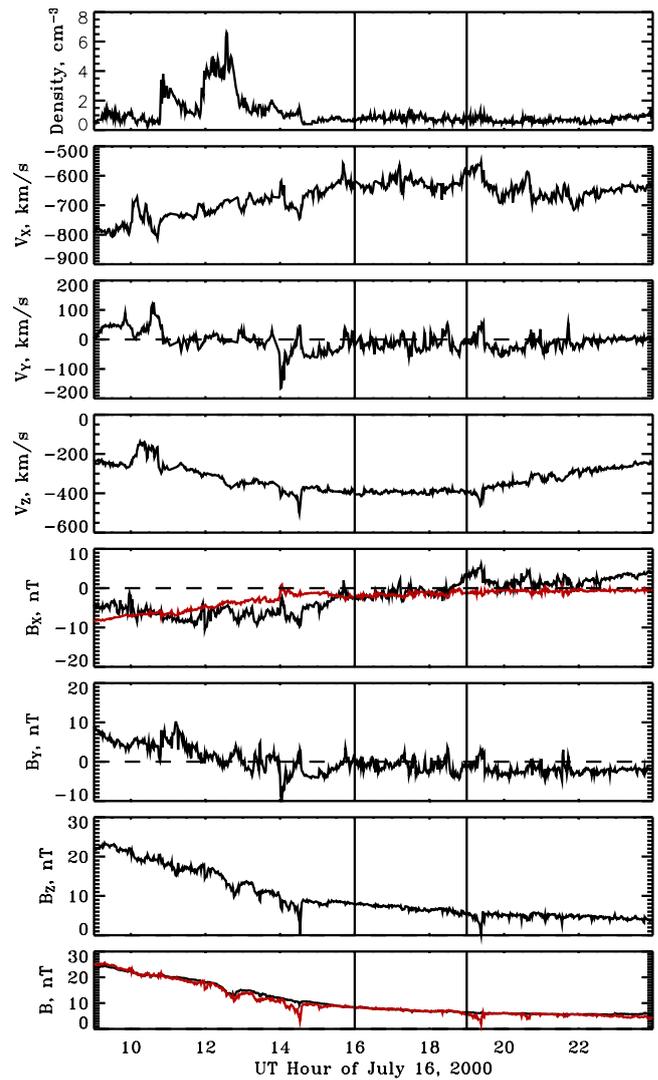
Fig. 1. Solar wind plasma and IMF data observed by ACE in SM coordinate system. The vertical lines at 16:00 UT and 19:00 UT denote the period during which comparisons are made. The red trace in the 5th panel shows $B_X = -0.2802\, B_Y - 0.2712\, B_Z$ and in the last panel – the corresponding total magnetic field. See text for details.

observations to infer the 3-D orientation of phase fronts in the solar wind (Weimer et al., 2002)). In the present study, to simplify the inflow boundary condition, we represent the time-variable solar wind B_X in the form with no constant term, $B_X^{(0)} = 0$, which corresponds to the magnetic field lying completely in the plane of the front. For the IMF conditions shown in Fig. 1, minimizing the standard root-mean-square function of $B_X - \alpha B_Y - \beta B_Z$ yields $\alpha = -0.2802$ and $\beta = -0.2712$; the resulting B_X component is shown in the 5th panel of Fig. 1 by the red trace. The corresponding total magnetic field is depicted by the red line in the bottom panel of the figure. The obtained fit for the B_X IMF component
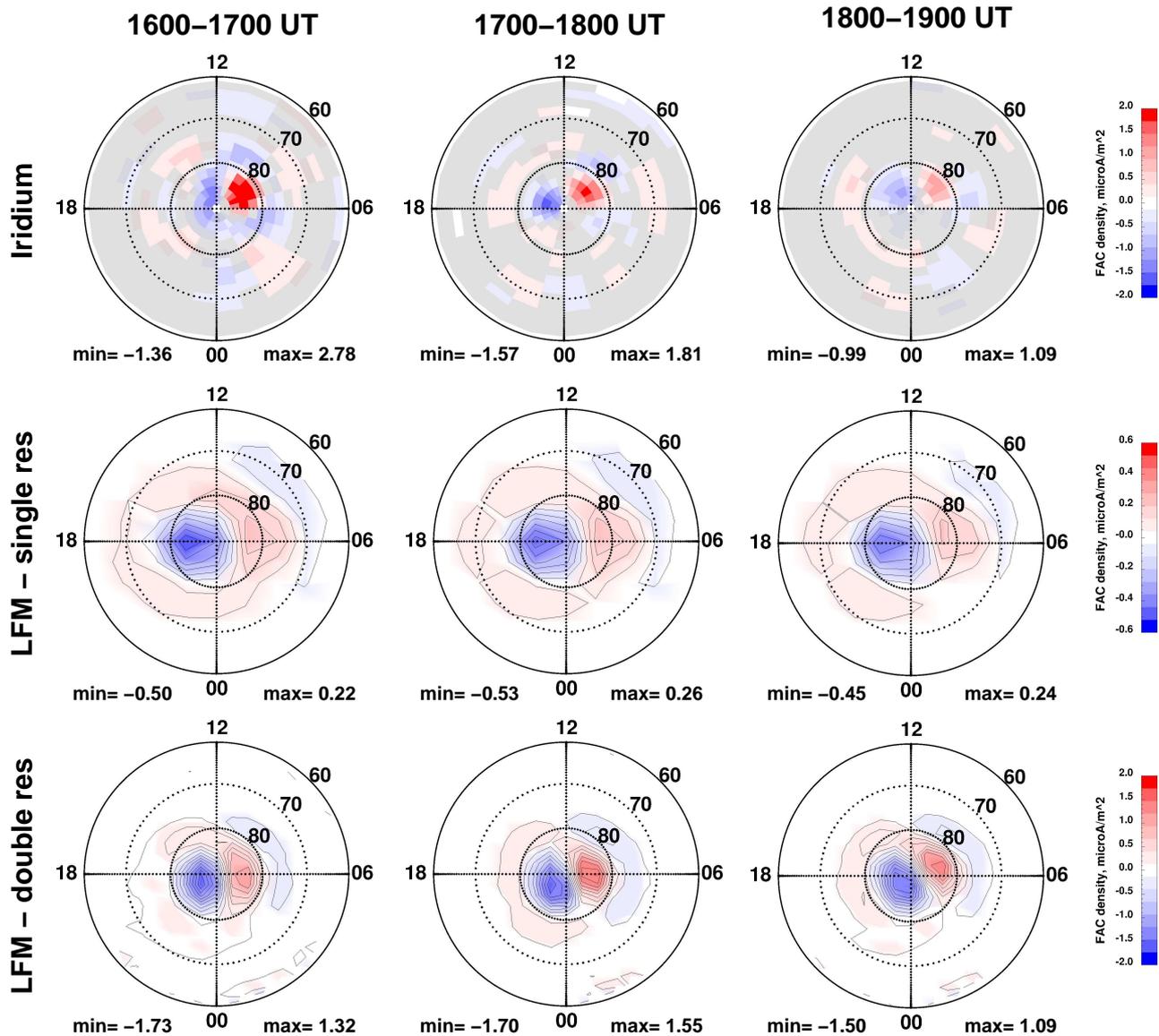
Fig. 2. One-hour average values of the Iridium (1st panel), single resolution LFM model (2nd panel), and double resolution LFM model (3rd panel) ionospheric field aligned current densities for the indicated hours during 16 July 2000. In Iridium plots, cells where the signal is within two standard deviations of zero are shaded gray.

agrees fairly well with the observed values during the period of interest, from 16:00 UT through 19:00 UT. However, there are still significant discrepancies between the observed and approximated magnetic field before 16:00 UT as well as at some times during the interval. For instance, for an extended period of time during the 18:00–19:00 UT hour the fitted B_X has the wrong sign.

4 Results

4.1 Ionospheric field aligned currents: comparison with Iridium

In this subsection we show comparisons of the simulated ionospheric field aligned currents with Iridium observations. Figure 2 displays the simulated and observed FAC density in the Northern Hemisphere. The field aligned current density inferred from the Iridium observations is shown in the first panel, while the second and the third panels show the current densities simulated by the single and double resolution LFM

model, respectively. The three columns correspond to three one-hour averages for the hours indicated: 16:00–17:00 UT, 17:00–18:00 UT, and 18:00–19:00 UT on 16 July 2000. The total integrated currents of the NBZ and Region 1 sense currents for these patterns are given in Table 1.

The comparison of the current distributions in the figure yields that increasing the simulation resolution leads to better agreement between the simulations and observations. The lower resolution simulation produces current (and electric field) structures that occupy a much larger area of the polar cap than are observed or obtained with the high resolution simulation. Note the factor of three difference in the color bar scales for the low and high resolution simulations. The current density in the low resolution run is considerably lower than either the high resolution run or the observations while the total currents of the low and high resolution runs are comparable. This reflects the larger area occupied by the currents in the low resolution run. The low resolution simulation looses some current due to the higher numerical diffusion, so that the discrepancy in the integrated field aligned currents between the low and high resolution simulations can reach a factor ∼2.

Focussing on the high resolution run, the comparison with the Iridium observations reveals that the LFM simulation captures the global structure of the field aligned currents fairly well. There is a significant NBZ current flowing poleward of 80° latitude and a weaker Region 1 sense current system between approximately 70° and 80° latitude. Comparatively minor discrepancies are evident including a slight shift of the current pattern toward the night side in the simulation, and that the simulated current features are larger in size than those observed by Iridium. The latter discrepancy is, as seen in Fig. 2, affected by the model resolution and therefore may be resolved by going to even higher resolution simulation.

The total current flowing in the indicated current systems provides a quantitative measure for comparison. Table 1 compares the integrated ionospheric current averaged over all three hours of interest (16:00–19:00 UT on 16 July 2000) as inferred from Iridium observations as well as simulated by the double-resolution LFM model. Korth et al. (2005) determined that Iridium-inferred magnetic perturbations (and therefore the field-aligned currents as well) were consistently lower than values observed by DMSP spacecraft. They introduced a numerical factor of 1.36 to correct for this discrepancy. In Table 1, the second row represents the uncorrected Iridium values presented by Korth et al. (2005), while the third row shows the values corrected by the above factor. The LFM-inferred NBZ currents are found by integrating the upward and downward current densities poleward of 80° boundary. Correspondingly, the Region 1 sense currents are assumed to be confined between 70° and 80° latitude. Examination of the 3rd panel in Fig. 2 confirms that this is a sufficiently good approximation suitable for our analysis. As seen in the table, the current distribution is slightly differ-

Table 1. Comparison of the integrated field aligned current (in MA) averaged from 16:00 UT to 19:00 UT on 16 July 2000 between Iridium and the double resolution LFM[a].

	NBZ+	NBZ−	R1+	R1−	Total
LFM double res	0.68	0.87	0.47	0.29	1.15
Iridium uncorrected	0.85	0.76	0.4	0.52	1.44
Iridium corrected	1.16	1.03	0.54	0.71	1.96

[a]"NBZ+" and "NBZ−" denote the upward and downward NBZ currents, respectively. Correspondingly, "R1+" and "R1−" stand for the upward and downward Region 1 sense currents. Iridium values are summarized as presented by Korth et al. (2005). Total current means either upward or downward current, the two being equal in magnitude.

ent in the simulations than Iridium observations: The LFM model produces a little less upward NBZ current and more downward NBZ current, while the situation is reversed in the case of the Region 1 sense current. The total current simulated by the LFM model is a factor of 1.25 smaller than the uncorrected Iridium value and about 1.7 times smaller than the corrected one. Here, the total current is found by summing up either upward or downward current, which in the case of the LFM yields a discrepancy between the total upward and downward currents of ∼0.1 MA. Considering the crudeness of our computation of the total current in the LFM simulation as well as the fact that Iridium did not rule out small Region 2 currents below 0.19 MA (upward) and 0.16 MA (downward) (Korth et al., 2005), Table 1 demonstrates a very good quantitative agreement of the ionospheric field aligned current between the LFM and the uncorrected Iridium values. As shown above, the underestimation of the LFM field-aligned current density compared to the corrected Iridium values can be to some extent resolved by a higher resolution simulation. In addition, in combination with the displacement of the FAC pattern it may be indicative of the difference between the simulated and actual solar wind magnetic field, particularly the B_X component, discussed in the previous section.

4.2 Ionospheric magnetic perturbations: comparison with DMSP

Another important signature of the magnetosphere-ionosphere coupling is the magnetic perturbations induced in the ionosphere by the field aligned currents flowing through the system. Magnetometers onboard DMSP spacecraft provide a separate measurement of the magnetic perturbations in addition to Iridium observations used in the previous section (the field aligned currents are derived from the magnetic perturbations actually measured by Iridium).

In order to compute magnetic field perturbations from the ionospheric field-aligned currents obtained from the LFM simulations, we apply the technique, which involves the separation of the divergenceless current and magnetic field into
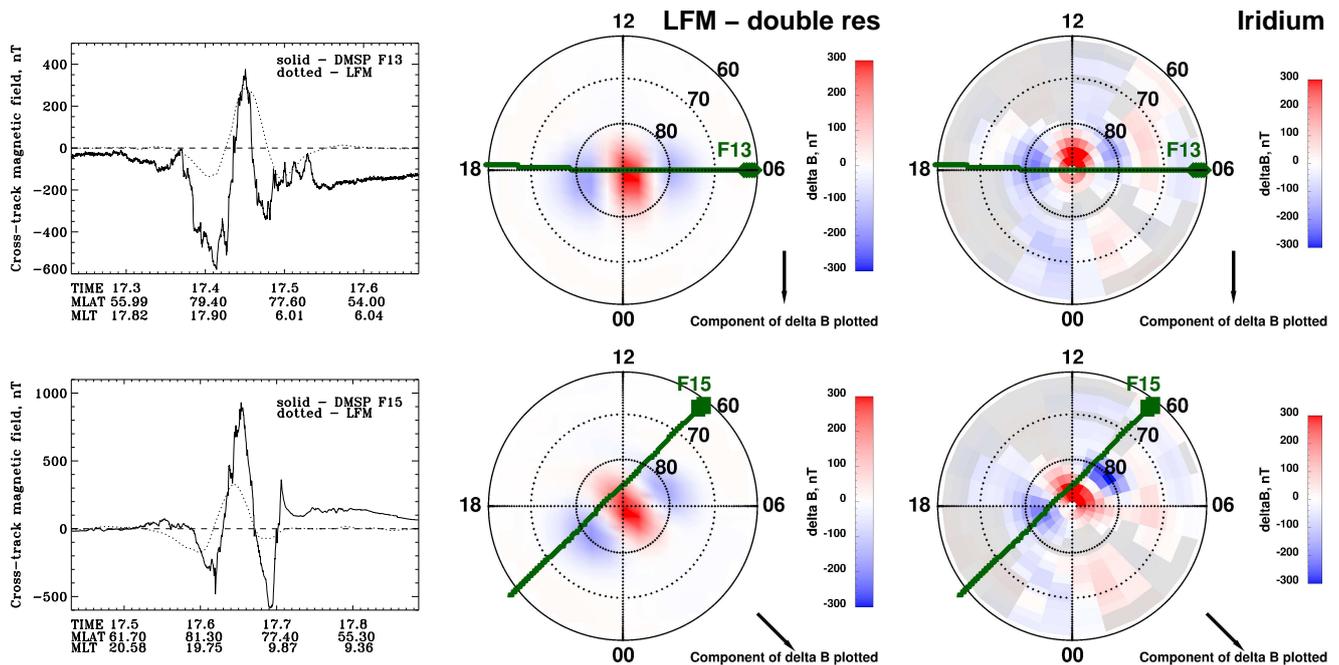
Fig. 3. Comparison of the cross-track magnetic perturbations measured by DMSP F13 (first panel) and F15 (second panel) satellites with double resolution LFM simulations for the polar passes during 17:14–17:40 UT and 17:26–17:53 UT, respectively. The polar plots in the second column show the satellite trajectories plotted over the LFM-simulated magnetic perturbation component in the direction shown in the bottom right corner of the plot (see text for details). The third column has the same format as the second one but the LFM-simulated magnetic perturbations are replaced by those inferred from Iridium observations. In Iridium plots, cells where the magnetic perturbation magnitude is within two standard deviations from zero are shaded gray.

the toroidal and poloidal components (Backus, 1986; Engels and Olsen, 1998). This technique (or its variations) has been used for reconstruction of ionospheric FACs from magnetic field perturbations observed by Magsat (Olsen, 1997), Iridium (Waters et al., 2001), and DE2 (Weimer, 2001) spacecraft. We essentially apply the inversion of this procedure as presented by (Weimer, 2001). First, the poloidal scalar is obtained by solving Poisson's equation:

$$J_\| = \frac{1}{\mu_0} \Delta_\perp \Psi, \tag{6}$$

where $J_\|$ is the simulated ionospheric FAC, Ψ is the poloidal scalar for the current (same as the toroidal scalar for the magnetic field), and $\Delta_\perp$ is the transverse part of the Laplacian operator in spherical coordinates. Equation (6) is solved using the same algorithm that is applied for the solution of the magnetosphere-ionosphere coupling equation in the LFM simulation code (Lyon et al., 2004). The magnetic field perturbation created by the FAC above is then given by

$$\delta\mathbf{B} = \hat{\mathbf{r}} \times \nabla_\perp \Psi, \tag{7}$$

where $\hat{\mathbf{r}}$ is the unit vector in the radial direction and $\nabla_\perp$ is the transverse component of the gradient. The limitation of the procedure above is that the field-aligned current is assumed

to be radial, a reasonable approximation, considering that we are concerned here with ionospheric signatures of the high-latitude NBZ current system. In order to make comparisons with DMSP and Iridium spacecraft observations the magnetic perturbations from the LFM model are mapped along the field lines according to $r^{3/2}$ scaling. These comparisons are presented next.

In Fig. 3, the line plots in the first column show the comparisons of the cross-track magnetic perturbations measured by F13 (upper plot) and F15 (bottom plot) DMSP satellites during their northern polar passes, at times marked on the horizontal axes of the plots, and the corresponding values determined from the LFM simulations (dotted line). The comparisons with either of the satellites appear to be discouraging at the first sight. The basic W-shaped feature corresponding to the NBZ current system is reproduced by the simulation (cf. comparisons with the Iridium FACs), but the magnitudes of the simulated quantities are significantly lower than the DMSP observations, except the middle peak on the F13 satellite line plot, which is matched fairly well.

Some of the discrepancies seen on the line plots in Fig. 3 are readily understood when the DMSP track is considered relative to the simulated and Iridium distributions of magnetic perturbations in the cross-track direction. Plots in the

2nd and 3rd columns in Fig. 3 show the distributions of the magnetic perturbations in the DMSP F13 (top) and F15 (bottom) cross-track directions from the simulations (middle) and the Iridium observations (right). Since the cross-track component of the magnetic perturbations is defined only locally at the satellite position, we choose a horizontal component of the simulated perturbations that is approximately perpendicular to the satellite trajectory at every point. We also note that the Iridium magnetic perturbations in this figure are not corrected by the 1.36 factor. The upper plot in the 2nd column in Fig. 3 shows the SM negative x-component of the LFM simulated ionospheric magnetic perturbations averaged from 17:00 UT to 18:00 UT, with the satellite trajectory plotted on top of it. The trajectory lies to a good accuracy in the dawn-dusk meridional plane and therefore the magnetic perturbation component plotted is mostly perpendicular to the trajectory. Similarly, the bottom plot in the 2nd column shows the SM negative (x+y)-component as indicated by the black arrow in the lower right corner of the plot.

The polar plots in the 2nd and 3rd columns in the figure demonstrate that most gross features of the global distribution of magnetic perturbations are well reproduced by the simulation, and the amplitudes of most peak values match fairly well the uncorrected Iridium observations (cf. FAC comparisons in Fig. 2). Therefore, there are two reasons for the seemingly poor agreement between the LFM model and DMSP observations, seen in the line plots in the 1st column. Firstly, it is due partly to the fact that in the model the field aligned current and magnetic perturbations are somewhat displaced and rotated. For instance, for the F15 polar pass the second negative structure around 17:40 UT is practically not captured by the simulation at all (see the bottom plot in the first column), but the polar plot shows that this results from the fact that the corresponding simulated structure is rotated out of the satellite trajectory, and the virtual satellite flown through the simulation just skirts the noon-side edge of the structure. Thus, rather than showing that the simulations fail to capture an important current system, the DMSP comparison is consistent with the displacement toward the nightside of the dawnside currents in the simulation. Secondly, considering the good overall agreement of LFM and Iridium distributions of magnetic perturbations (Fig. 3, 2nd and 3rd columns) and the fact that the uncorrected Iridium data (Fig. 3, 3rd column) underestimate magnetic perturbations (Korth et al., 2005), and assuming that the ionospheric convection pattern inferred from Iridium observations has the correct geometry, we conclude that in addition to the displacement in the LFM results, the LFM magnetic perturbations are underpredicted compared to the DMSP data, which is in agreement with our FAC comparison (see Sect. 4.1).

4.3 Ionospheric plasma drift velocity and electrostatic potential pattern: comparison with DMSP

This subsection compares the ionospheric plasma drift velocities with DMSP F13 and F15 measurements. Figure 4 demonstrates the point made in the previous section. Panels (a) and (b) show the cross-track drift velocities measured by the drift meters onboard DMSP F13 and F15 satellites (solid trace) along with those inferred from the double resolution LFM simulations, whereby the electric field along the track of the satellite is obtained from the ionospheric part of the simulation and crossed with the dipole magnetic field to compute the cross-track velocity. The polar plot (c) depicts the spatial structure of the LFM-simulated ionospheric electrostatic potential, satellite tracks overplotted.

Figure 4 demonstrates that the LFM simulation underestimates the ionospheric convective electric field owing, to a large extent, to geometrical factors. The virtual DMSP F13 satellite passes exactly through the minimum of the simulated potential, and the corresponding dip in the cross-track velocity around 17:30 UT is reproduced surprisingly well (once the satellite passes through the minimum of the potential, the cross-track velocity changes the sign from positive to negative). On the other hand, the satellite does not see the maximum of the potential, and therefore neither the first dip in the cross-track velocity (∼17:25 UT) nor the peak are captured well. The F15 virtual satellite does pass close to the maximum of the potential, but not close enough, so that there is a substantial track-aligned drift velocity component. Finally, it misses completely the minimum of the potential, and thus almost no second dip in the cross-track velocity.

Even accounting for the displacement of the convection cells in the LFM the simulation underestimates the potentials. Korth et al. (2005) estimate the maximum potential measured among the two DMSP satellites during the mentioned polar passes to be about +27 kV. The corresponding minimum potential is −15 kV, so that the transpolar potential is not less than +42 kV. The LFM-simulated value averaged from 17:00 UT to 18:00 UT is +28 kV. There are three factors that affect the simulation convection intensity. First, the LFM grid resolution affects numerical diffusion in the code and leads to a spreading of the currents such that the potentials are further separated in the ionosphere in the lower resolution run. This leads to a lower electric field simply by virtue of the greater distance between extrema in the potential. The low resolution run, using the same ionospheric conductance yields only half the potential of the high resolution run showing that the potential difference is also lower due to grid resolution, mostly likely due to a reduction in the reconnection intensity due to numerical diffusion. Thus, a still higher resolution simulation may yield a higher potential. The conductance also affects the potential. Below in Sect. 4.6 we compare the low resolution simulation for different ionospheric conductance models and find that the more realistic conductance, which in the region of interest is lower,
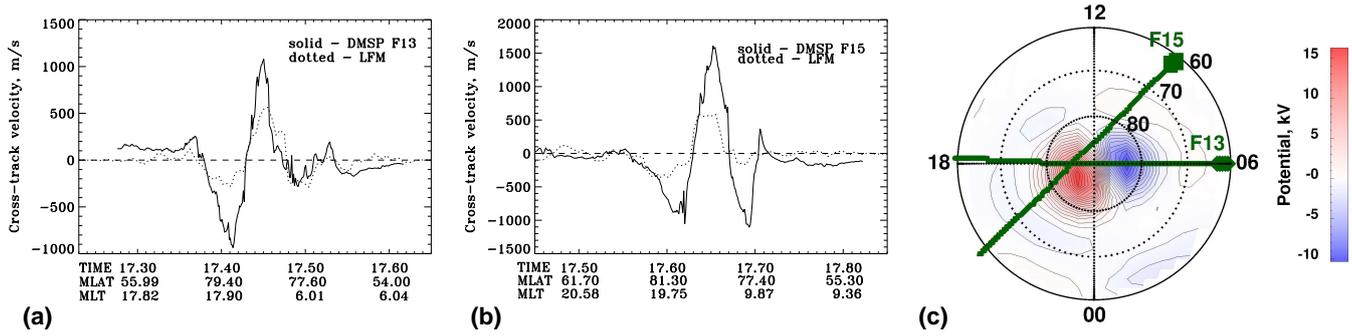
Fig. 4. Comparison of the cross-track drift velocity measured by DMSP F13 **(a)** and F15 **(b)** satellites with double resolution LFM simulations for the polar passes during 17:14–17:40 UT and 17:26–17:53 UT, respectively. The polar plot **(c)** shows the LFM-simulated Northern Hemisphere electrostatic potential pattern, averaged from 17:00 UT to 18:00 UT, with the satellite trajectories overplotted.

yields a higher potential. This is likely simply due to Ohms law since the total currents with the different conductances are the same. Thus, the current deficit is not resolved by the conductance model improvement.

Finally, we noted before that the underestimation of the LFM field-aligned current density compared to the Iridium data, corrected to obtain the best fit to the DMSP measurements, may be due to the reconnection efficiency being too low in the simulation owing to an inaccurate representation of the three-dimensional structure of the IMF. The latter would result in a lower simulated transpolar potential as well. The comparison of the DMSP and LFM transpolar potentials yields (see above) 42/28=1.5, which is similar to the factor of 1.7 obtained for the discrepancy of the field-aligned currents between the LFM and corrected Iridium. The effect of the IMF orientation is discussed further in Sect. 5.

4.4 Poynting flux: comparison with Iridium

The Poynting flux into the ionosphere is determined by the convective electric field and magnetic perturbations:

$$\mathbf{S} = \frac{1}{\mu_o}\mathbf{E} \times \delta\mathbf{B}. \tag{8}$$

Having calculated the magnetic perturbation $\delta\mathbf{B}$ in Sect. 4.2 and using the electric field $\mathbf{E}$ results presented in Sect. 4.3, we are now able to calculate the Poynting flux $\mathbf{S}$ directly. However, for the purposes of comparison with the Iridium estimate (Korth et al., 2005), it is not necessary. Indeed, to obtain that estimate Korth et al. (2005) approximated the electric field as

$$\mathbf{E} = \frac{1}{\mu_0\Sigma_P}\hat{\mathbf{r}} \times \delta\mathbf{B}, \tag{9}$$

which is equivalent to the neglect of conductance gradients and the neutral wind in the ionosphere. Under these assumptions, Eq. (9) follows from the fact that the poloidal scalar Ψ

is proportional to the ionospheric electrostatic potential Φ, which is found by solving (e.g. Lyon et al., 2004)

$$J_\parallel = \nabla_\perp(\mathbf{\Sigma}\nabla_\perp\Phi) \approx \Sigma_P\Delta_\perp\Phi, \tag{10}$$

where $\mathbf{\Sigma}$ is the conductance tensor and Σ_P is its diagonal term (Pedersen conductance). Provided the same boundary conditions are used for solving Eqs. (6) and (10), one obtains

$$\Psi = \frac{\Sigma_P\Phi}{\mu_0}, \tag{11}$$

which immediately yields Eq. (9), taking into account Eq. (7) and $\mathbf{E} = -\nabla_\perp\Phi$. Combining Eqs. (8) and (9) yields

$$\mathbf{S} = -\hat{\mathbf{r}}\left(\Sigma_P\mathbf{E}^2\right), \tag{12}$$

i.e. under the assumptions made, the local Poynting flux being equivalent to the local Joule heating (cf. Eqs. 3 and 5 in Korth et al., 2005). Our direct verification of Poynting flux $\mathbf{S}$ calculated according to Eq. (12) and (9) yields very minor differences for this particular simulation, which indicates that effects of conductance gradients are indeed small, and hence, to make our comparisons consistent with calculations by Korth et al. (2005), we apply Eq. (12) for the determination of the Poynting flux hereafter.

Figure 5 depicts the magnitude of the vector $\mathbf{S}$ in Eq. (12) with the same quantity determined from Iridium observations. It should be noted that this time the Iridium plot is based on the data corrected by Korth et al. (2005) to obtain the best comparison with DMSP data. Therefore, we do not expect an extremely good agreement between the corrected Iridium and the LFM results, considering the underestimation of both the field-aligned current (and therefore magnetic perturbations) and the convective electric field discussed above. While Fig. 5 shows that there is a significant difference in magnitude, the structure of the Poynting flux is very similar, keeping in mind that both the electric field and

magnetic perturbation patterns are somewhat displaced in the simulation with respect to Iridium data. The simulation reproduces the central region of intense flux, the two "voids" of energy flux associated with the NBZ currents, and the surrounding region of lower flux located between the NBZ and Region 1 sense currents. It should be noted that the integrated electromagnetic power input into the ionosphere is a better proxy for the comparison, since the Poynting flux in the simulations is spread over a wider area. The total power input estimated from Iridium data is 51 GW, while integration of the flux in Fig. 5b yields 16 GW.

From Eq. (12) it follows that the ionospheric Poynting flux (and the Joule heating) is defined by the Pedersen conductance and convective electric field. Therefore, given a fixed ionospheric conductance model, the Poynting flux quadratic dependence on the convective electric field (and magnetic perturbations) accounts for the factor of 3 underestimation of the LFM total electromagnetic input into the ionosphere. It should also be noted that in order to estimate the Poynting flux from Iridium observations Korth et al. (2005) had to adopt an ionospheric conductance model different from the one used in the LFM model. There is indeed some evidence that the ionospheric conductance is somewhat overestimated in the LFM simulation (see Sect. 4.6). Bearing in mind, that it is also indicated in that subsection that the better conductance model tends to increase the ionospheric electric field while not changing the field-aligned current significantly, we conclude that the use of a better conductance model would nudge the Poynting flux estimate in the right direction. This results from the fact that the magnetic perturbation is given by (see Eq. 9):

$$\delta \mathbf{B} = -\mu_0 \Sigma_P \hat{\mathbf{r}} \times \mathbf{E}, \tag{13}$$

and if we assume roughly that the field-aligned current and $\delta \mathbf{B}$ are not affected by the ionospheric conductance under the simulated conditions, the Poynting flux would increase linearly with the electric field. We note however that the ionospheric conductance is a relatively minor factor affecting the electromagnetic flux in the model during the simulated interval. It is the underestimation of the field-aligned currents and electric fields that accounts for the major discrepancy between the LFM and Iridium results.

4.5 Precipitating electron energy flux: comparison with IMAGE FUV

In this subsection we compare the precipitating electron energy flux estimated from the simulation results to the IMAGE FUV data presented by Korth et al. (2005). The intention is to test the empirical model of electron precipitation within the LFM simulation code under the conditions of weak magnetosphere forcing (northward IMF). The model relates the precipitating electron energy and number flux to MHD macrovariables at the inner boundary of the MHD simulation (Fedder et al., 1995b).
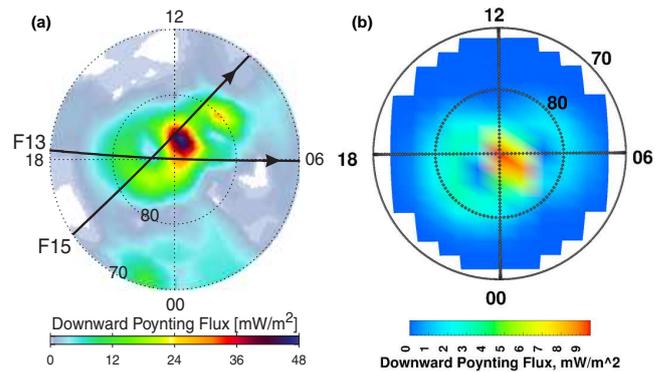
Fig. 5. Comparison of the radial Poynting flux in the Northern Hemisphere between Iridium (**a** – adapted from Korth et al., 2005) and double resolution LFM (**b**) from 17:00 UT to 18:00 UT.

Figure 6 shows the comparison in the same format as Fig. 5. The peak of the precipitating electron energy flux is displaced in the simulation compared to the IMAGE FUV data, which is a direct consequence of the fact that the simulated upward NBZ current is displaced, as has been shown in Sect. 4.1. Quantitatively, the LFM model clearly underestimates the precipitating energy flux as well as the integrated energy deposition by about an order of magnitude (0.55 GW versus 6 GW for the IMAGE FUV estimate according to Korth et al. (2005)). An interesting point to make here is that the peak characteristic energy of the precipitating electrons is actually overestimated by the LFM simulation (3.3 keV versus 750 eV – obtained by Korth et al. (2005) based on DMSP data). The problem here is not the discrepancy between the simulations and observations per se, but rather the fact that the model overestimates the electron energy and underestimates the energy and number fluxes at the same time. Indeed, the model performance is governed by a few empirical coefficients that can be tuned to the simulated conditions. We therefore consider whether it is possible to accomplish the tuning in such a way that would reconcile both the electron energy and number flux.

Turning to the formalism (1–5), suppose a triple of coefficients $\{\alpha_1, \beta_1, R_1\}$ yields $\{E_1, \Phi_1\}$ for the particle energy and flux. We seek a triple $\{\alpha_2, \beta_2, R_2\}$ that would decrease the flux and yet increase the energy: $\Phi_2 = q_\Phi \Phi_1$ and $E_2 = q_E E_1$, where $q_\Phi < 1$ and $q_E > 1$. Clearly, the answer depends strongly on the value of the exponent in Eq. (5), which in turn is determined by the relation between $E_\parallel$ and E_0. We can, however, see whether the triple $\{\alpha_2, \beta_2, R_2\}$ exists in the two limiting cases: $E_\parallel \gg E_0$ and $E_\parallel \ll E_0$. The results of this simple estimate are as follows:
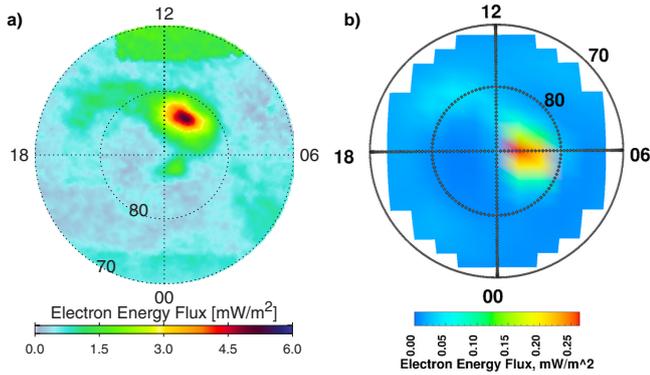
Fig. 6. Comparison of the precipitating electron energy flux in the Northern Hemisphere between Iridium (**a** – adapted from Korth et al., 2005) and double resolution LFM (**b**) from 17:00 UT to 18:00 UT.

1. $E_\parallel \gg E_0$

$$q_\Phi = \frac{\beta_2}{\beta_1}\sqrt{\frac{\alpha_2}{\alpha_1}}$$

$$q_E = \frac{R_2}{R_1}\sqrt{\frac{\alpha_2}{\alpha_1}},$$

2. $E_\parallel \ll E_0$

$$q_\Phi = \frac{\beta_2}{\beta_1}\sqrt{\frac{\alpha_2}{\alpha_1}}$$

$$q_E = \frac{\alpha_2}{\alpha_1}.$$

Thus, the condition $q_\Phi q_E \sim \gamma$ yields

$$\frac{\alpha_2\beta_2 R_2}{\alpha_1\beta_1 R_1} \sim \gamma, \text{ in the first limit}$$

and

$$\frac{\alpha_2^{3/2}\beta_2}{\alpha_1^{3/2}\beta_1} \sim \gamma, \text{ in the second limit,}$$

where γ is a constant describing the discrepancy in the particle energy and flux. In the above case, for instance, $\gamma \sim 1/10$ since the energy flux is underpredicted by an order of magnitude, while the energy is overpredicted by a factor of ~ 4, which means that the number flux is underestimated by a factor of ~ 40, so that $q_\Phi \sim 1/40$, $q_E \sim 4$, and $q_\Phi q_E \sim 1/10$. Clearly, both above conditions can be satisfied by proper tuning of the coefficients. Of course, this tuning should be performed in such a way that keeps the $E_\parallel/E_0 \gg 1$ or $\ll 1$ limits intact.

The above simple estimate gives us some confidence in that an adjustment of the coefficients is possible for any relation between $E_\parallel$ and E_0. Therefore, the poor performance of

the LFM model of the precipitating particle energy and flux under conditions of week magnetosphere forcing can be improved by proper tuning of the empirical coefficients. Given the flexibility of the parameters to match a given set of observations, it still remains to consider whether any specific set of parameters is generally applicable. Assessing this question requires analysis of multiple events.

We can however consider how much difference the precipitation estimate makes for the simulation results in this case. We do not expect it to make a large difference, since the precipitating particles seemingly do not affect the ionospheric conductance, at least in the case presented. Indeed, Korth et al. (2005) discussed that during the event considered here, the Northern Hemisphere is almost totally sunlit (large dipole tilt), which explains the domination of the EUV ionization over the precipitation. Therefore, the underestimation of the precipitating particle energy flux in the simulation is not expected to affect significantly the ionospheric conductance. The performance of the precipitation model during weak driving in general deserves a separate study and therefore will not be discussed here any further.

4.6 Standalone LFM and CMIT simulations

In this subsection the results of the standalone LFM simulations are compared to the coupled LFM/TING (CMIT) model simulations. As mentioned above, the coupled model can be run only in the single resolution at this time. The comparisons above were made using the double resolution standalone LFM simulations. Therefore, we will not compare the results of the coupled simulation to the observations. Rather, they will be compared to a standalone single resolution LFM simulation, to explore how much of the discrepancy in the predicted ionospheric field aligned current and convection pattern can be accounted for by the ionospheric conductance model.

Figure 7 presents the results of these simulations in the following format. The first panel shows the standalone LFM simulation results averaged over the three hours between 16:00 UT and 19:00 UT on 16 July 2000. The 1st, 2nd, and 3rd columns depict the ionospheric field aligned current, electrostatic potential, and Pedersen conductance, respectively. The 2nd panel shows the same quantities simulated using the CMIT model. As the polar plots in the 1st column show, the field aligned current remains practically unaffected by the change of the ionospheric conductance model. This suggests that the simulated magnetosphere-ionosphere system operates close to the current-generator mode under the simulated conditions. This, in turn, implies that the ionospheric conductance model cannot explain discrepancies between the simulated field aligned current pattern and Iridium observations.

The ionospheric conductance does affect the ionospheric electrostatic potential and convective electric field. Column 2 of Fig. 7 displays the electrostatic potential simulated by the
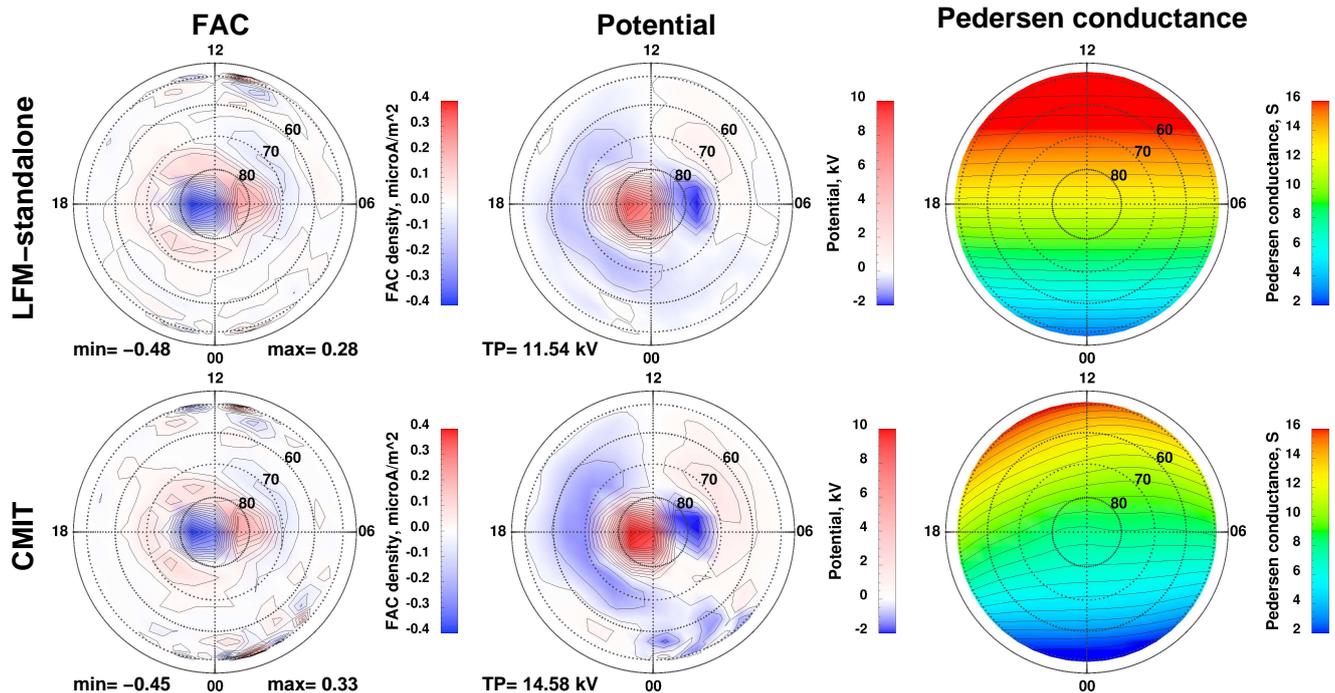
Fig. 7. Three-hour average (16:00–19:00 UT on 16 July 2000) values of the ionospheric field aligned current (1st column), electrostatic potential (2nd column), and Pedersen conductance (3rd panel) of the standalone single resolution LFM (1st panel) and CMIT (2nd panel) simulations.

two models considered here. Clearly, the geometry of the convection pattern remains unchanged when the ionospheric conductance model within the LFM simulation code is replaced by the TING model, but the magnitude of the potential is increased, since TING yields a somewhat lower Pedersen (and Hall) conductance (see the plots in the 3rd column of Fig. 7). The transpolar potential changes from $\sim$12 kV for the standalone LFM to $\sim$15 kV for the CMIT simulation. This result suggests that the quantitative discrepancy between the observed and simulated convection velocity and electric field discussed in Sect. 4.3 is partly due to the ionospheric conductance being too low in the simulation. Although the increase of 3 kV in the transpolar potential, accounted for by using the TING conductances instead of the standalone LFM values, might seem insignificant, it constitutes 25% of the original value. Hence we conclude that the use of the better conductance model does nudge the electrostatic potential solution in the direction towards a better agreement with observations, albeit it alone cannot explain the discrepancies between the LFM simulation and observations.

5 Discussion and summary

We presented results of global MHD simulations of an event with sustained northward IMF previously examined by Korth et al. (2005) using data from Iridium spacecraft. Our primary purpose here was to test the performance of the LFM global MHD model during conditions of weak magnetosphere driving. We have used Iridium constellation data for comparisons of the ionospheric field aligned current pattern as well as the magnetometer and drift meter data from DMSP satellites for comparisons of ionospheric magnetic perturbations and convection velocities. In addition, results published by Korth et al. (2005) are used for the comparison of the simulated and observed flux and precipitating electron energy flux into the ionosphere.

The results of these comparisons are summarized below.

5.1 Field aligned currents

The global MHD simulation captures main features of the ionospheric field aligned current pattern during northward IMF: There is a pronounced NBZ current system poleward of 80° magnetic latitude (this is resolution dependent, however) and a weaker Region 1 sense current system at lower latitudes. The current magnitude is dependent on the simulation resolution so that the comparisons improve with increasing

resolution. The total amount of current flowing through the system shows a good agreement with Iridium when the LFM simulations are completed at a high enough resolution. However, if the Iridium results are corrected to obtain the best fit to the DMSP observations (see Korth et al., 2005, for details) the LFM currents turn out to be about 1.7 times smaller than the modified Iridium values. Combined with the slight displacement of the simulated field-aligned current pattern toward the night side, this suggests that an inaccurate description of the three-dimensional structure of the IMF in the simulations (see Sect. 3) may be the cause of this behavior. Indeed, it is known that for simulations of idealized solar wind conditions with due northward IMF and strictly anti-sunward solar wind flow, the LFM model (Fedder et al., 1995a) as well as other global MHD models (Song et al., 1999; Vennerstrom et al., 2005) place the NBZ current system more towards the day side consistent with Iridium observations. Another piece of information comes from the LFM simulation we have accomplished that was completely identical to the one described above except the IMF B_X component was set to zero. That simulation revealed the average field-aligned current and electrostatic potential patterns similar to the ones presented here but the magnitudes of those quantities were consistently smaller. These two facts combined indicate that the slight displacement of the simulated ionospheric convection pattern and the underestimation of the field-aligned currents and electric fields may be related and result from the imposed reconnection flows being too low due to inaccurate representation of the three-dimensional structure of the IMF in the simulation. We conclude that the magnitude of the IMF B_X component may be very important during weakly driven conditions simulated here and its effect on the geometry and efficiency of reconnection occurring above the cusps in global MHD models should be studied in more detail.

Finally, the CMIT model simulations demonstrate that the ionospheric conductance model does not affect the field aligned current pattern significantly as the simulated magnetosphere-ionosphere system operates close to the current-generator mode under these conditions.

5.2 Magnetic perturbations

As a separate check on the representation of the field aligned currents in the simulations, magnetic perturbations derived from FACs in the simulations were compared to the cross-track magnetic perturbations measured by magnetometers onboard DMSP F13 and F15 satellites. We showed that the observed discrepancies are to a large extent due to the displacement of the FAC pattern. This led us to conclude that single satellite comparisons are insufficient for simulation validation. Independent measurements from multiple satellites used to derive global estimates of electrodynamic parameters are required to make a sensible assessment of the model performance. The global distribution of the FACs and magnetic perturbations obtained from Iridium enabled us to make such quantitative evaluation of the global MHD model.

5.3 Plasma drift velocity and electric field

The geometrical factors described above cannot fully account for the underprediction of the convection velocities and electric fields (and potential) compared to the DMSP spacecraft single point observations. This is demonstrated by the simulated transpolar potential being consistently smaller than the lower limit given by DMSP observations. The accompanying underestimation of the field-aligned current density in the simulations suggests that the reconnection efficiency is too low as discussed above. In addition, CMIT simulations show that a better conductance model improves the electric field pattern although it is not the primary factor under the simulated conditions. Finally, a higher simulation resolution is shown to increase the ionospheric convective electric field considerably. It seems likely, though it remains to be demonstrated, whether these three factors can bring the LFM electric field upto the level observed by the DMSP. We note also, that the underestimation of the strength of the ionospheric convection and field-aligned currents in this simulation is important to recognize, especially, in view of the well-known notion that global MHD models usually overpredict these quantities represented, for instance, by the cross-polar cap potential, during events driven by the southward IMF. The distinction is clearly in the orientation of the IMF and is likely to be related to the numerical representation of magnetic reconnection above the cusp as opposed to the subsolar magnetopause.

5.4 Poynting flux

The total electromagnetic flux input into the ionosphere is underestimated by a factor of ∼3 in the simulation as compared to the Iridium estimate (we note, however, that Korth et al., 2005, evaluate the error of their calculation to be ∼20%). Taking into account the fact that both the ionospheric field-aligned current and electric field are lower than observed values by a factor of roughly 1.5–2 this is not surprising. As discussed above we identify three major sources of these discrepancies. Firstly, the simulation resolution affects the field-aligned current as well as the electric field so that these quantities increase with increasing resolution. Secondly, the IMF orientation (in particular, the magnitude of B_X) are important in determining the location and efficiency of the magnetopause reconnection. Lastly, the better ionospheric conductance model is shown to nudge the solution for the simulated ionospheric electric field and hence the Poynting flux towards a better agreement with observations.

5.5 Precipitating particle energy and flux

Poor performance of the model of particle precipitation within the LFM model is explained by the need to tune

empirical coefficients governing the behavior of the model to the simulated conditions (northward IMF– weak magnetosphere driving). We showed in Sect. 4.5 that according to the analytical expressions underlying the model, such tuning is possible. Additional validation studies are required to determine the proper values for the coefficients and determine whether a given set of coefficients can be identified that apply under general conditions. In addition, it is to be understood whether precipitation is relevant at all under the presented conditions. In the case under the consideration here, for instance, the ionospheric conductance is completely dominated by the EUV ionization, and the electron precipitation, although miscalculated, does not affect the result of the simulation at all.

5.6 Summary

In summary, we find that the LFM global MHD model performed well under the conditions of weak driving. The morphology of the simulated ionospheric convective pattern agrees with observations. The accurate description of the three-dimensional structure of the IMF is an important factor determining the location and efficiency of the magnetopause reconnection in the simulation and therefore it affects the geometry and intensity of the ionospheric convective pattern. In addition, the quantitative discrepancies found can be partly eliminated by improving the model resolution and the ionospheric conductance model, for example, by performing simulations using the LFM coupled to an ionosphere-thermosphere model.

References

Anderson, B. J., Takahashi, K., and Toth, B. A.: Sensing global Birkeland currents with Iridium® engineering magnetometer data, Geophys. Res. Lett., 27, 4045–4048, 2000.

Anderson, B. J., Takahashi, K., Kamei, T., Waters, C. L., and Toth, B. A.: Birkeland current system key parameters derived from Iridium observations: Method and initial vaidation results, J. Geophys. Res., 107, 1079, doi:10.1029/2001JA000080, 2002.

Backus, G.: Poloidal and toroidal fields in geomagnetic field modeling, Rev. Geophys., 24, 75–109, 1986.

Burke, W. J., Kelley, M. C., Sagalyn, R. C., Smiddy, M., and Lai, S. T.: Polar cap electric field structures with a northward interplanetary magnetic field, Geophys. Res. Lett., 6, 21–24, 1979.

Chiu, Y. T. and Cornwall, J. M.: Electrostatic model of a quiet auroral arc, J. Geophys. Res., 85, 543–556, 1980.

Chiu, Y. T., Newman, A. L., and Cornwall, J. M.: On the structures and mapping of auroral electrostatic potentials, J. Geophys. Res., 86, 10 029–10 037, 1981.

Engels, U. and Olsen, N.: Computation of magnetic fields within source regions of ionospheric and magnetospheric currents, J. Atmos. Solar-Terr. Phys., 60, 1585–1592, 1998.

Fedder, J. A. and Lyon, J. G.: The earth's magnetosphere is 165 R_E long: Self-consistent currents, convection, magnetospheric structure, and processes for northward interplanetary magnetic field, J. Geophys. Res., 100, 3623–3635, 1995.

Fedder, J. A., Lyon, J. G., Slinker, S. P., and Mobarry, C. M.: Topological structure of the magnetotail as function of interplanetary magnetic field direction, J. Geophys. Res., 100, 3613–3621, 1995a.

Fedder, J. A., Slinker, S. P., Lyon, J. G., and Elphinstone, R. D.: Global numerical simulation of the growth phase and the expansion onset for substorm observed by Viking, J. Geophys. Res., 100, 19 083–19 093, 1995b.

Fridman, M. and Lemaire, J.: Relationship between auroral electrons fluxes and field aligned electric potential difference, J. Geophys. Res., 85, 664–670, 1980.

Ijima, T., Potemra, T. A., Zanetti, L. J., and Bythrow, P. F.: Large-scale Birkeland currents in the dayside polar region during strongly northward IMF: A new Birkeland current system, J. Geophys. Res., 89, 7441–7452, 1984.

Korth, H., Anderson, B. J., Wiltberger, M. J., Lyon, J. G., and Anderson, P. C.: Intercomparison of ionospheric electrodynamics from the Iridium consttellation with global MHD simulations, J. Geophys. Res., 109, A07307, doi:10.1029/2004JA010428, 2004.

Korth, H., Anderson, B. J., Frey, H. U., and Waters, C. L.: High-latitude electromagnetic and particle energy flux during an event with sustained strongly northward IMF, Ann. Geophys., 23, 1295–1310, 2005,
http://www.ann-geophys.net/23/1295/2005/.

Lyon, J. G., Fedder, J. A., and Mobarry, C. M.: The Lyon-Fedder-Mobarry (LFM) global MHD magnetospheric simulation code, J. Atmos. Solar-Terr. Phys., 66, 1333–1350, doi:10.1016/j.jastp.2004.03.020, 2004.

Olsen, N.: Ionospheric *F* region currents at middle and low latitudes estimated from Magsat data, J. Geophys. Res., 102, 4563–4576, 1997.

Raeder, J., McPherron, R. L., Frank, L. A., Kokubun, S., Lu, G., Mukai, T., Paterson, W. R., Sigwarth, J. B., Singer, H. J., and Slavin, J. A.: Global simulation of the Geospace Environment Modeling substorm challenge event, J. Geophys. Res., 106, 381–395, 2001.

Robinson, R. M., Vondrak, R. R., Miller, K., Babbs, T., and Hardy, D. A.: On calculating ionospheric conductivities from the flux and energy of precipitating electrons, J. Geophys. Res., 92, 2565–2569, 1987.

Song, P., DeZeeuw, D. L., Gombosi, T. I., Groth, C. P. T., and Powell, K. G.: A numerical study of solar wind-magnetosphere interaction for northward interplanetary magnetic field, J. Geophys. Res., 104, 28 361–28 378, 1999.

Vennerstrom, S., Moretto, T., Rastatter, L., and Raeder, J.: Field-aligned currents during northward interplanetary magnetic field: Morphology and causes, J. Geophys. Res., 110, A06205, doi:10.1029/2004JA010802, 2005.

Wang, W., Killeen, T. L., Burns, A. G., and Roble, R. G.: A high-resolution, three-dimensional, time dependent, nested grid model of the coupled thermosphere-ionopshere, J. Atmos. Solar-Terr. Phys., 61, 385–397, 1999.

Wang, W., Wiltberger, M., Burns, A. G., Solomon, S. C., Killeen, T. L., Maruyama, N., and Lyon, J. G.: Initial results from the coupled magnetosphere-ionosphere-thermosphere model: thermosphere-ionosphere responses, J. Atmos. Solar-Terr. Phys., 66, 1425, doi:10.1016/j.jastp.2004.04.008, 2004.

Waters, C. L., Anderson, B. J., and Liou, K.: Estimation of global field aligned currents using the Iridium® system magnetometer data, Geophys. Res. Lett., 28, 2165–2168, 2001.

Weimer, D. R.: Maps of ionospheric field-aligned currents as a function of the interplanetary magnetic field derived from Dynamics Explorer 2 data, J. Geophys. Res., 106, 12 889–12 902, 2001.

Weimer, D. R., Ober, D. M., Maynard, N. C., Burke, W. J., Collier, M. R., McComas, D. J., Ness, N. F., and Smith, C. W.: Variable time delays in the propagation of the interplanetary magnetic field, J. Geophys. Res., 107, 1210, doi:10.1029/2001JA009102, 2002.

Wiltberger, M., Wang, W., Burns, A. G., Solomon, S. C., Lyon, J. G., and Goodrich, C. C.: Initial results from the coupled magnetosphere-ionosphere-thermosphere model: magnetospheric and ionospheric responses, J. Atmos. Solar-Terr. Phys., 66, 1411, doi:10.1016/j.jastp.2004.03.026, 2004.

Zanetti, L. J., Potemra, T. A., Ijima, T., Baumjohann, W., and Bythrow, P. F.: Ionospheric and Birkeland current distributions for northward interplanetary magnetic field: Inferred polar convection, J. Geophys. Res., 89, 7453–7458, 1984.